

Discrete-Time Fourier Series to Simulate Transient Overvoltages in Power Systems

Arash Tavighi, Hamed Ahmadi, Mažana Armstrong, José R. Martí

Abstract—This paper presents a methodology based on the Discrete-Time Fourier Series (DTFS) to calculate transient overvoltages in power systems. The proposed algorithm determines the time window with sufficient width to allow the time constants of the transients to decay to a small value. This method is simpler than the traditional numerical Laplace transform (NLT) and does not require parameter adjustment to obtain very accurate results. The test case is based on a study to calculate Transient Over-Voltage (TOV) for 138 kV transmission lines in British Columbia, Canada. To assess the accuracy of the results, the DTFS solution is compared with the traditional NLT solution with optimized parameters and with the EMTP frequency dependent time domain models fdLINE and ULM.

Keywords—Discrete-Time Fourier Series, Numerical Laplace Transform, electromagnetic transient simulation.

I. INTRODUCTION

TRANSIENT Over-Voltages (TOV) can be a safety hazard for live-line/bare-hand work in the right-of-way of overhead transmission lines. BC Hydro initiated studies to confirm that historically used limits of approach distances, also known as the Minimum Approach Distance (MAD), are still adequate for their system. In order to calculate MAD for a given transmission line according to the IEEE Std. 516TM [1], the maximum switching surge overvoltage needs to be calculated. The main purpose of this study is to calculate the TOVs generated due to line energization and fault incidents using frequency-domain solutions.

Frequency-domain methods solve electromagnetic transients directly in the frequency domain and transfer the solution from frequency to time using numerical Fourier or Laplace transforms. These methods do not rely on curve-fitting approximations as opposed to frequency-dependent transmission line models in the EMTP [2], such as the fdLINE model [3] and the ULM [4]. As a result, frequency-domain solutions constitute valuable tools to verify the solutions for time-domain frequency-dependent transmission lines [5]–[11].

The Numerical Laplace Transform (NLT) has been traditionally used for frequency-domain solutions of power system transients [12]–[15]. However, the NLT requires an experienced user to specify the value of the damping factor to make sure the transients of the signal are contained inside the

time window of the study and filtering windows to eliminate aliasing and Gibbs oscillations. When bringing the signal back to time, the use of a boosting factor to compensate for the damping factor often results in amplifying the Gibbs oscillations [15]. The use of the well-known windowing functions to reduce these errors may not be totally effective since it corrupts the few initial samples of the simulation [16].

A simple methodology based on the Discrete-Time Fourier Series (DTFS) was introduced in [16]. Guidelines to use this methodology were also presented in [16]. The main concept is to allow all transients of interest to die out inside the chosen time window width. The frequency window width is selected according to the maximum frequency desired to be captured in the transient (as done in the traditional EMTP). By allowing the transient to naturally die out inside the time window, there is no need for arbitrary compression and decompression factors like in the NLT and accuracy and integrity of the signals is preserved. The size of the time window in the DTFS is calculated as the sum of the simulation time and largest time constant of the system. The time constants can be obtained using eigenvalues analysis.

In terms of solution speeds, the NLT uses odd sampling [16], while the DTFS can use regular sampling. This results in twice the number of operations for the NLT for the same number of sampling points. In the simulations in this paper, the results with the normally used time window for the NLT were less accurate than those with the DTFS and we had to increase this time window for comparable results, thus giving a further solution time disadvantage for the NLT as compared with the DTFS.

The DTFS gave very accurate results for the AC interference test of asymmetrical transmission lines with nearby objects [17], and for the switching transient of double-circuit lines [18]. This paper presents simplified guidelines with respect to [16] for practical engineering applications. We also present a larger test case than those of [18]. This test case involves different line configurations and conductor types, bundled conductors, shield wires, various line lengths and soil resistivity values, and asymmetrical short-circuit conditions.

II. POWER SYSTEM TRANSIENT SOLUTION USING THE DISCRETE-TIME FOURIER SERIES (DTFS)

Frequency-domain solutions use nodal analysis to solve the system one frequency at a time,

$$\mathbf{V}(\omega) = \mathbf{Y}(\omega)^{-1}\mathbf{I}(\omega) \quad (1)$$

where \mathbf{V} is the calculated node voltages, \mathbf{Y} is the matrix of admittances, and \mathbf{I} is the injected current sources.

This research has been supported from a Mitacs grant in Canada.

Arash Tavighi and José R. Martí are with the Electrical and Computer Engineering Department, University of British Columbia, Vancouver, Canada (emails: arashtav@ece.ubc.ca, jrms@ece.ubc.ca). Hamed Ahmadi and Mažana Armstrong are with the Transmission Line Electrical Design, BC Hydro, Burnaby, Canada (emails: hamed.ahmadi@bchydro.com, mazana.armstrong@bchydro.com).

Paper submitted to the International Conference on Power Systems Transients (IPST2019) in Perpignan, France June 17-20, 2019.

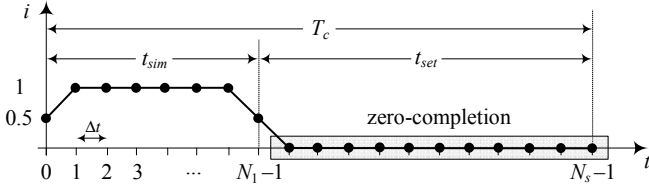


Fig. 1. Time window selection for the DTFS.

To solve (1) in the frequency domain, we use the DTFS to convert the injected current sources from time to frequency,

$$I[k] = \frac{1}{N_s} \sum_{n=0}^{N_s-1} i[n] e^{-jk \frac{2\pi}{N_s} n} = DTFS\{i[n]\} \quad (2)$$

The number of sample points is $N_s = T_c f_c$, where T_c is the width of the time window and f_c is the width of the frequency window. After solving (1), we use the Inverse Discrete-Time Fourier Series (IDTFS) to convert the node voltages from frequency to time to form the transient response,

$$v[n] = \sum_{k=\lfloor -\frac{N_s-1}{2} \rfloor}^{\lceil \frac{N_s-1}{2} \rceil} V[k] e^{jk \frac{2\pi}{N_s} n} = IDTFS\{V[k]\} \quad (3)$$

where $\lceil \cdot \rceil$ and $\lfloor \cdot \rfloor$ are the ceiling and floor functions, respectively. For these conversions, the DTFS requires to define a time window T_c and a frequency window f_c .

A. Time-window Width (T_c)

Figure 1 shows the time window selection for an example discrete-time current source applied to a system for a simulation time t_{sim} with N_1 samples. The rest of sequence for the source (up to $N_s - 1$) is completed by adding sample points with zero value (“zero completion”). This portion of the time window corresponds to settling time t_{set} where the response of the system to the last sample of the source decays to a small value.

The width of T_c must be sufficient to include the observation time of the simulation t_{sim} plus the time required for the transients to die out after the source is applied t_{set} [16],

$$T_c = t_{sim} + t_{set} \quad (4)$$

Since we stop the source at t_{sim} , a snapshot of t_{sim} will be the final time-domain solution. The rest of the samples in the time window are auxiliary points which should be discarded. The simulation time t_{sim} is specified by the user, while the settling time t_{set} can be chosen as a factor of the slowest mode of the system τ_m ,

$$t_{set} = k_{set} \tau_m \quad (5)$$

In [16] k_{set} was recommended as 7 so that all transient components of the time response to decay to less than 0.1% of their initial value ($e^{-7} \approx 10^{-3}$). However, for power systems’ applications $k_{set} = 3$ has been found to be sufficient to achieve accurate results.

The time constants of a circuit with lumped-elements can be determined by extracting the poles of the corresponding transfer function. In general, this can be achieved using many available routines such as *linmod* in MATLAB/Simulink.

Assume that the poles for a stable system of order n are,

$$p_i = \alpha_i \pm j\beta_i \quad , \quad i = 1, 2, \dots, n \quad (6)$$

The largest time constant of the system τ_m is

$$\tau_m = \frac{1}{\min(-\alpha_i)} \quad (7)$$

Figure 1 shows that for the first and last samples, the average of the values before applying the source and after applying the source can be used to improve the accuracy of the DTFS at discontinuities [19].

B. Frequency-window Width (f_c)

The width of the frequency window f_c is determined by the maximum frequency of the transient. The maximum frequency that can be captured in the solution is f_{Ny} (Nyquist frequency),

$$f_c = 2f_{Ny} = \frac{1}{\Delta t} \quad (8)$$

For a system described by its poles as in (6), the highest harmonic in the transient is associated with the imaginary part of the poles β ,

$$f_{Ny} = \frac{\max(|\beta_i|)}{2\pi} \quad (9)$$

For power systems applications, we have observed that the resolution associated with the real part of the poles α is either below the value given in (9) or corresponds to transients that decay very fast. An exception to this is for systems of order one (e.g., R-L circuit) where $f_{Ny} = \max(-\alpha_i)$ will provide the required resolution for the decaying exponential. The resolution given by (9) is also adequate for the common sources in power systems (e.g., sinusoidal, decaying exponential, and step function). If higher resolutions are desired, f_{Ny} can be augmented by a waveform resolution factor discussed in [16].

C. Other Simulation Parameters

Once T_c and f_c have been chosen, the number of sample points N_s is determined by

$$N_s = T_c f_c \quad (10)$$

For non-integer values, N_s in (10) is rounded up. The time step size and the frequency step size are given by

$$\Delta t = \frac{T_c}{N_s} \quad , \quad \Delta f = \frac{f_c}{N_s} \quad (11)$$

The DTFS can work equally well for regular sampling ($\omega = 2\pi n \Delta f$) and for odd sampling ($\omega = \pi (2n + 1) \Delta f$) for $n = 0, 1, 2, \dots, N_s - 1$. The use of regular sampling is preferred to increase the computational efficiency by a factor of two using the complex conjugate property [16].

III. APPLICATION OF THE DTFS TO SIMULATE FREQUENCY-DEPENDENT TRANSMISSION LINES

For an N -phase frequency-dependent transmission line with a given geometry and ground return parameters, the admittance matrix in (1) can be calculated using a coupled exact- π circuit. To form the exact- π circuit, the per-unit-length line series impedance matrix \mathbf{Z}_{ph} and shunt admittance matrix \mathbf{Y}_{ph} are calculated from the Line Constants routine in EMTP packages such as EMTP-RV and PSCAD.

To calculate the elements of π -circuits, \mathbf{Z}_{ph} and \mathbf{Y}_{ph} are transferred from coupled phase quantities to decoupled modal quantities using modal transformation matrices,

$$\mathbf{Z}_m = \mathbf{T}_V^{-1} \mathbf{Z}_{ph} \mathbf{T}_I, \quad \mathbf{Y}_m = \mathbf{T}_I^{-1} \mathbf{Y}_{ph} \mathbf{T}_V \quad (12)$$

In (12), \mathbf{T}_V diagonalizes $\mathbf{Z}_{ph} \mathbf{Y}_{ph}$ and \mathbf{T}_I diagonalizes $\mathbf{Y}_{ph} \mathbf{Z}_{ph}$. To compensate for the distributed nature of the line parameters, the modal impedances and admittances in (12) are corrected for the line length ℓ and the frequency by applying the factors k_z and k_y of (14):

$$Z'_m = k_z Z_m \ell, \quad Y'_m = k_y Y_m \ell \quad (13)$$

$$k_z = \frac{\sinh(\gamma_m \ell)}{\gamma_m \ell}, \quad k_y = \frac{\tanh\left(\frac{\gamma_m \ell}{2}\right)}{\frac{\gamma_m \ell}{2}} \quad (14)$$

where γ_m is the modal constant of propagation,

$$\gamma_m = \sqrt{Z_m Y_m} \quad (15)$$

The exact- π circuit in the phase domain can now be calculated by transferring \mathbf{Z}'_m and \mathbf{Y}'_m from mode to phase,

$$\mathbf{Z}'_{ph} = \mathbf{T}_V \mathbf{Z}'_m \mathbf{T}_I^{-1}, \quad \mathbf{Y}'_{ph} = \mathbf{T}_I \mathbf{Y}'_m \mathbf{T}_V^{-1} \quad (16)$$

The largest time constant τ_m and the maximum frequency f_{Ny} for frequency-dependent transmission lines can be approximated as follows:

- 1) We calculate \mathbf{Z}_{ph} and \mathbf{Y}_{ph} at low frequencies (e.g., 60 Hz) from the Line Constants routine in the EMTF. The shunt conductance G_{ins} can be neglected due to its minor impact on τ_m and f_{Ny} .
- 2) We assume that the line is transposed, and we can use the symmetrical components values to calculate the zero/positive/negative sequence series impedances and shunt admittances,

$$Z^o = Z_s + (N - 1) Z_m, \quad Z^+ = Z^- = Z_s - Z_m \quad (17)$$

$$Y^o = Y_s + (N - 1) Y_m, \quad Y^+ = Y^- = Y_s - Y_m$$

In (17), subscript s refers to the average of the diagonal elements whereas subscript m is the average of the off-diagonal elements of the \mathbf{Z}_{ph} and \mathbf{Y}_{ph} . The positive and negative sequence networks have the same time constants.

- 3) We use (13) to calculate the zero/positive sequence parameters of the equivalent π -circuits. Since the correction factors k_z and k_y in (13) are close to one at low frequencies, we can further simplify the procedures by skipping (14) and (15).
- 4) We connect the zero/positive sequence π -circuits to the rest of the system components and assume receiving-end terminals are all shorted.
- 5) We use (7) and (9) to calculate τ_m and f_{Ny} for the equivalent sequence networks.

The validity of approximations such as taking \mathbf{Z}_{ph} and \mathbf{Y}_{ph} at low frequency, *transposed lines*, and *shorted terminals* was verified in [16]. The validity of assuming k_z and k_y as one and ignoring G_{ins} will be discussed in IV.

The parameters calculated with the described procedure are sufficient for the margins required in determining the largest time constant and the maximum frequency.

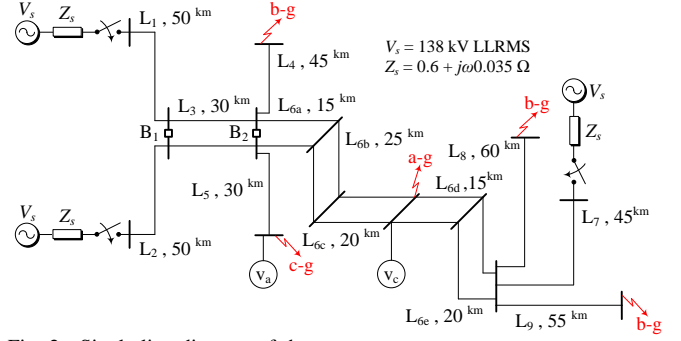


Fig. 2. Single-line diagram of the test case.

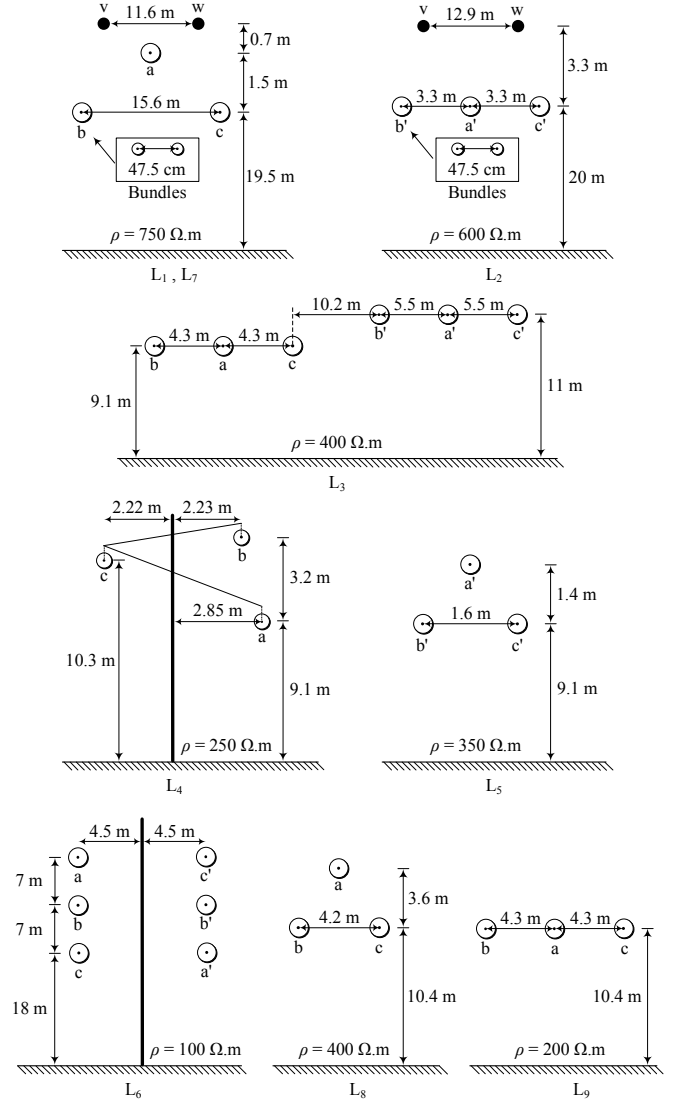


Fig. 3. Geometries and configurations of conductors for the lines in Fig. 2.

IV. TEST CASE

The test case includes nine transmission lines of different length as shown in Fig. 2. The configurations, geometries and values of soil resistivity of the lines are indicated in Fig. 3.

The conductor arrangements are based on the common configurations for 138 kV lines used in BC Hydro system. The double-circuit vertical line L_6 is split into 5 segments. The lines L_1 , L_2 , and L_7 include bundled conductors and shield wires. In British Columbia, transmission lines are not shielded, except for a short section outside the substations. The main

TABLE I
DIAMETER, DC RESISTANCE, AND THICKNESS RATIO FOR CONDUCTORS
IN FIG. 3.

Lines	d (cm)	R_{DC} (Ω/km)	Ratio
L ₁ , L ₂ , L ₇ (a-b-c)	2.8143	0.0702	0.32
L ₁ , L ₂ , L ₇ (v-w)	0.9144	4.1592	0.50
L ₃	1.8313	0.1660	0.32
L ₄ , L ₈	1.6307	0.2090	0.32
L ₅	2.0117	0.1336	0.50
L ₆	2.9591	0.0590	0.375
L ₉	2.1780	0.1170	0.32

TABLE II
THE LARGEST TIME CONSTANTS τ_m AND THE MAXIMUM FREQUENCIES
 f_{Ny} OF THE TEST CASE IN FIG. 2 FOR DIFFERENT CONDITIONS.

k_z, k_y	G_{ins} (S/km)	τ_m^0 (s)	τ_m^+ (s)	f_{Ny}^0 (kHz)	f_{Ny}^+ (kHz)
$\neq 1$	2×10^{-9}	0.05631	0.06619	27.4333	39.4742
$= 1$	2×10^{-9}	0.05642	0.06620	27.4322	39.4734
$\neq 1$	0	0.05684	0.06659	27.4333	39.4742
$= 1$	0	0.05682	0.06658	27.4322	39.4734

reasons for this consideration are the low isokeraunic levels and the natural shielding provided by the trees [20].

The line conductors are untransposed and sagging is neglected. The diameter, DC resistance, and thickness ratio of the conductors of Fig. 3 are given in Table I. The value of the insulator losses G_{ins} is taken as 2×10^{-9} S/km [11].

The lines are connected to a balanced three-phase voltage source and the peak value of phase-a is applied at $t = 0$. The equivalent source impedance corresponds to the impedance of the generator plus its step-up transformer. Circuit breakers B₁, B₂ are normally open.

Terminal conditions are considered as a line-to-ground fault in various buses (resistance of $10^{-6}\Omega$ for shorted and $10^6\Omega$ for open). A line-to-ground fault happens on phase-a of L_{6d}. This condition produced the maximum TOV for this simulation.

Due to space limitation, the outputs are given only for the receiving-end phases that show the largest discrepancies. Scope v_a shows the maximum TOV generated in phase-a, where v_c indicates higher harmonics in phase-c of the associated buses.

The π -circuit parameters for the lines of Fig. 3 were calculated at 60 Hz. From this circuit, for the zero sequence and positive sequence parameters, the network poles are extracted using eigenvalue analysis. The poles are then used to calculate τ_m and f_{Ny} , as given in Table II. This table also shows the negligible impact of assuming $k_z, k_y = 1$ and $G_{ins} = 0$ on τ_m and f_{Ny} .

V. SIMULATION CONDITIONS

The DTFS and the NLT algorithms were programmed in MATLAB, the fdLINE model was run using EMTP-RV v3.5, and the ULM was run using PSCAD v4.5.2. The simulation settings for the different solutions are presented next.

A. DTFS Simulation Setup

Table III shows the procedures to calculate the time-frequency parameters for the DTFS based on the guidelines of Sections II and III.

TABLE III
TIME-FREQUENCY PARAMETERS FOR THE DTFS.

User			Base		Derived		
t_{sim} (s)	τ_m (s)	f_{Ny} (Hz)	T_c (s)	f_c (Hz)	N_s	Δf (Hz)	Δt (μs)
0.1	0.067	39474	0.3	78948	23684	3.33	12.67

First, the user specifies the desired simulation time t_{sim} . Then the slowest time constant τ_m and the maximum frequency f_{Ny} are calculated using (7) and (9), respectively for the equivalent zero/positive sequence networks of Fig. 2. Next, the base parameters T_c and f_c are determined from the knowledge of user parameters. As discussed in Section II, the time window T_c is calculated as $t_{sim} + 3\tau_m$ using (4) and the frequency window f_c is chosen as $2f_{Ny}$ using (8). As also discussed, the simulation with the DTFS will be valid from 0 to t_{sim} . Finally, other simulation parameters N_s , Δf , Δt are derived from the base parameters using (10) and (11).

For the DTFS regular sampling was used and no windowing function is needed. To avoid division by zero when taking the inverse of \mathbf{Y} in (1), the DC frequency was taken as 10^{-4} Hz.

B. NLT Simulation Setup

The NLT was implemented using the conventional instructions as given in [15]. The setup is as follows.

Damping factors: Wilcox criterion σ_1 [12], Wedepohl criterion σ_2 [13], Error criterion σ_3 ($\epsilon = 10^{-4}$) [14].

Sampling schemes: Regular sampling and odd sampling.

Windowing functions: Lanczos. Similar to [16], Hanning and Tukey windows gave similar results as Lanczos.

Time window: Three settings were considered for T_c : a) $1.1t_{sim} = 0.11$ s, b) $t_{sim} + 3\tau_m = 0.3$ s, c) 0.9 s.

The width $T_c = 0.11$ s corresponds to the most recommended setting for the NLT [8] [15]. For this setup, the T_c is chosen based on the size of the simulation time t_{sim} and an extra 10% extension to eliminate the Gibbs at signal's tail. $T_c = 0.3$ s is the recommended setting for the DTFS in this paper and is used for comparison. $T_c = 0.9$ s is the minimum required size of the time window for the NLT which gave correct results for the test case of this paper.

Frequency window: for comparison purposes the same f_c and Δt was chosen for the NLT as for the DTFS and the EMTP line models. The rest of the parameters N_s and Δf were calculated using (10) and (11).

C. fdLINE and ULM Simulation Setup

For comparison purposes, the same t_{sim} and Δt were used for the EMTP line models as for the DTFS method.

For the curve-fitting processes of fdLINE and ULM, the maximum number of poles was set to 35, and the frequency range was set from 10^{-2} to 10^7 Hz with 10 points per decade. For fdLINE, the transformation matrices were calculated using the automatic option.

VI. SIMULATION RESULTS

In this section, the solution obtained with the proposed DTFS is compared with NLT, fdLINE, and ULM.

A. Comparison of DTFS and NLT

Figures 4 to 6 show the simulation results for the open voltage v_a for the test case of Fig. 2 comparing the DTFS and the NLT. In Figs. 4 to 6, the top figure corresponds to the NLT with regular sampling and the bottom figure corresponds to the NLT with odd sampling. In all figures, the DTFS is implemented using $T_c = t_{sim} + 3\tau_m = 0.3$ s, regular sampling, and as discussed previously, no windowing function is needed.

Figure 4 compares the results for the NLT with the recommended setting $T_c = 1.1t_{sim} = 0.11$ s. As shown in this figure, the results obtained with the NLT with the recommended T_c did not converge to a correct solution. For both regular and odd sampling, the NLT deviated from the DTFS starting at about 0.02 s of simulation. In Fig. 4-top, the NLT gave NaN error (indeterminate value) in MATLAB for regular sampling with σ_3 . Gibbs errors were higher for regular sampling than odd sampling.

Next, the simulation condition in Fig. 4 for the NLT was repeated with the T_c recommended for the DTFS, i.e., $T_c = t_{sim} + 3\tau_m = 0.3$ s. Figure 5 compares the solutions obtained with the DTFS and the NLT for $T_c = 0.3$ s.

Figure 5 illustrates that increasing the size of T_c from 0.11 s to 0.3 s reduced the Gibbs oscillations for the NLT. However, numerical errors still exist, more prominently at the tail of the waveform. In this simulation σ_1 and σ_3 for odd sampling gave better results but still there is not a very good match. Similarly to the results of Fig. 4, the NLT with σ_2 produced stronger Gibbs oscillations, and the NLT with σ_3 and regular sampling gave NaN errors for which no output was produced.

To obtain correct results using the NLT, the simulation condition of Fig. 5 was repeated with T_c varied from 0.4 s for increments of 0.1 s. The minimum width of T_c for the NLT which gave correct results was 0.9 s. For the width of T_c from 0.4 s to 0.9 s, the NLT either gave erroneous outputs as reported in [10] [16], or did not produce any outputs (NaN errors). In contrast to the NLT, the proposed DTFS gave correct results for all widths of T_c from 0.3 s on.

Figure 6 repeats the simulation of Fig. 5 using $T_c = 0.9$ s for the NLT. As it can be observed, increasing the width of T_c to 0.9 s can suppress the Gibbs errors using odd sampling with σ_1 and σ_2 . For this setup, the NLT matched the DTFS, but at a higher computational cost (about six times, 32':42'' vs. 5':40''). The NLT with regular sampling and σ_2 had a minor vertical shift compared to the DTFS, and the NLT with σ_3 and σ_1 with regular sampling gave NaN errors.

B. Comparison of DTFS and NLT with the EMTP Line Models

Figure 7 compares open voltages v_a and v_c obtained with the proposed DTFS, NLT, fdLINE, and ULM for a transient period of 0.05 s for the test case of Fig. 2.

The simulation setup for the DTFS was $T_c = 0.3$ s, regular sampling, and no windowing function, whereas for the NLT was $T_c = 0.9$ s, odd sampling, σ_1 , and Lanczos window.

The results of Fig. 7 indicate that the DTFS and the NLT (after increasing its time window) match very well fdLINE and ULM. Some minor differences exist between the EMTP line models and the frequency-domain solutions, more noticeably

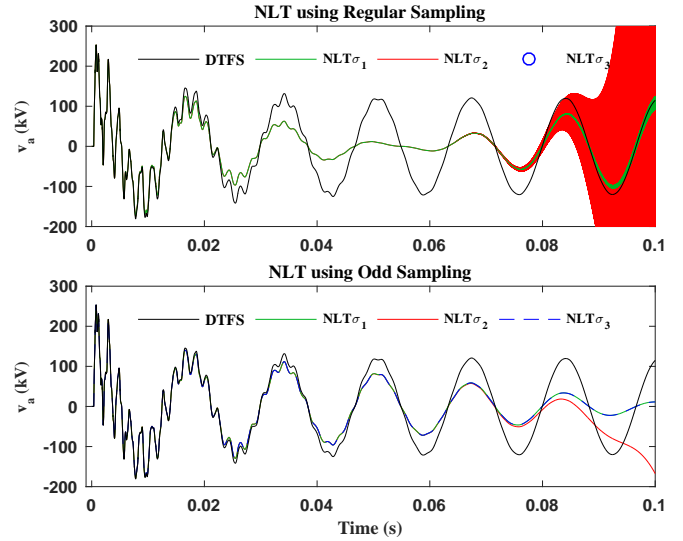


Fig. 4. Comparison of DTFS and NLT for v_a in the test case of Fig. 2. $T_c = 0.3$ s for the DTFS and $T_c = 0.11$ s for the NLT as recommended.

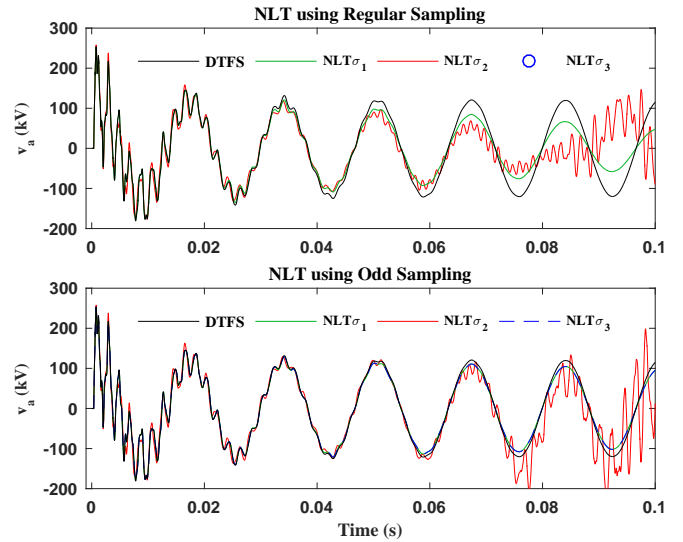


Fig. 5. Comparison of DTFS and NLT for v_a in the test case of Fig. 2. $T_c = 0.3$ s for the DTFS and the NLT.

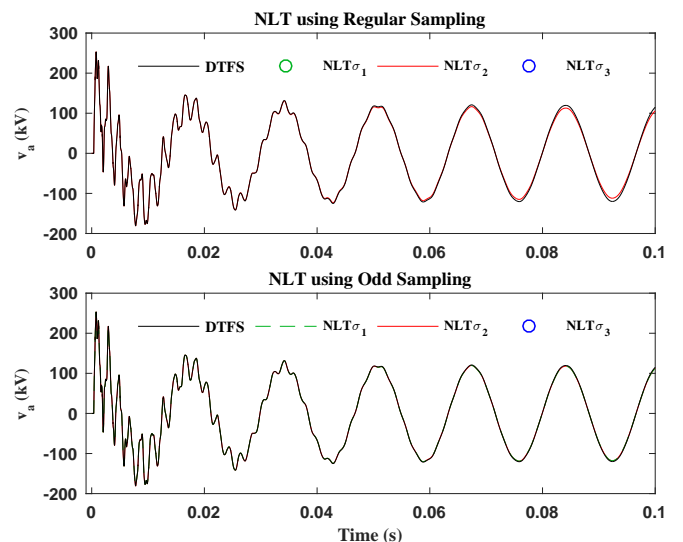


Fig. 6. Comparison of DTFS and NLT for v_a in the test case of Fig. 2. $T_c = 0.3$ s for the DTFS and $T_c = 0.9$ s for the NLT.

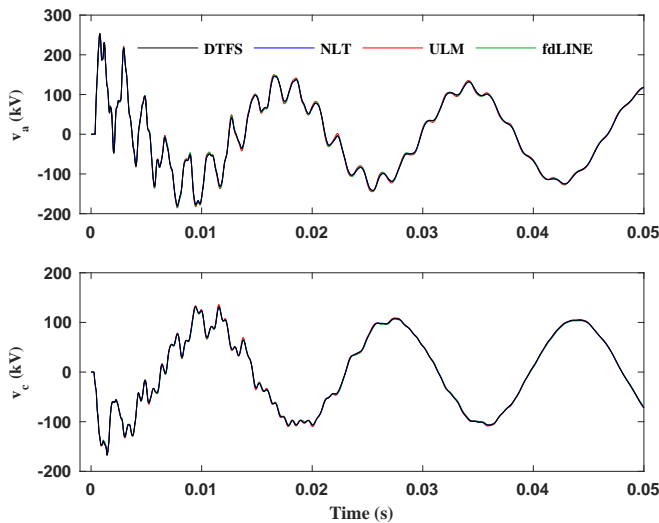


Fig. 7. Comparison of DTFS and NLT with fdLINE and ULM for v_a and v_c in the test case of Fig. 2. For the DTFS $T_c = 0.3$ s, regular sampling, and no filtering window. For the NLT $T_c = 0.9$ s, odd sampling, σ_1 , and Lanczos.

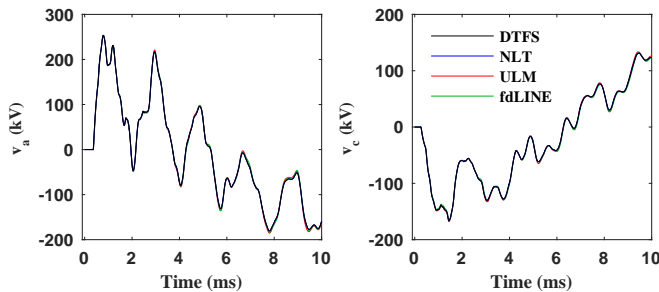


Fig. 8. Snapshot for the initial 10 ms of the simulation of Fig. 7.

in the jagged points of the waveforms. These small differences can be better observed in the snapshots of Fig. 8 for the initial 10 ms of the simulations. The reason for such discrepancies may be related to the curve-fitting approximations in the EMTP time-domain models. Maximum differences of solutions for the peak of TOV in Fig. 8-left is 0.35% in 253 kV.

VII. CONCLUSION

This paper uses the Time-Window-Based Discrete-Time Fourier Series (DTFS) to simulate transient over-voltages in power systems. The basis of this method is to capture the transient response of the system within the width of the chosen time window.

Unlike the NLT, the DTFS does not require using damping/boosting factors or filtering windows, which simplifies and increases its usability.

Despite the compression provided by the damping factor for the NLT, following the common practice of taking the simulation time as the width of the time window was not sufficient to include all the transient response. In the tests in this paper, the minimum time window width required by the NLT was three times larger than the required time window width the DTFS. This factor and the requirement of odd sampling made the NLT computationally more expensive than the DTFS.

The simulation results also showed that the time-domain line models in the EMTP, fdLINE and ULM, are very accurate.

High accuracy, low computational cost, and simplicity in the implementation make the proposed DTFS a general-purpose reliable tool for frequency-domain electromagnetic transient simulations.

REFERENCES

- [1] *IEEE Std. 516, IEEE guide for maintenance methods on energized power lines*, IEEE, NY, 2009.
- [2] H. W. Dommel, *Electromagnetic Transients Program (EMTP) Theory Book*, Sep. 1992.
- [3] J. R. Martí, "Accurate modelling of frequency-dependent transmission lines in electromagnetic transient simulations," *IEEE Trans. Power App. Syst.*, vol. PAS-101, no. 1, pp. 147–157, Jan. 1982.
- [4] A. Morched, B. Gustavsen, and M. Tartibi, "A universal model for accurate calculation of electromagnetic transients on overhead lines and underground cables," *IEEE Trans. Power Del.*, vol. 14, no. 3, pp. 1032–1038, Jul. 1999.
- [5] F. J. Marcano and J. R. Martí, "Idempotent line model: Case studies," in *Proc. Int. Conf. Power System Transients (IPST'97)*, Seattle, USA, 22–26 Jun. 1997, pp. 67–72.
- [6] H. V. Nguyen, H. W. Dommel, and J. R. Martí, "Direct phase-domain modelling of frequency-dependent overhead transmission lines," *IEEE Trans. Power Del.*, vol. 12, no. 3, pp. 1335–1342, Jul. 1997.
- [7] F. Castellanos and J. R. Martí, "Full frequency-dependent phase-domain transmission line model," *IEEE Trans. Power Syst.*, vol. 12, no. 3, pp. 1331–1339, Aug. 1997.
- [8] P. Moreno, P. Gómez, J. L. Naredo, and L. Guardado, "Frequency-domain transient analysis of electrical networks including non-linear conditions," *Int. J. Elect. Power Energy Syst.*, vol. 27, no. 2, pp. 139–146, Feb. 2005.
- [9] P. Gómez and F. A. Uribe, "The numerical Laplace transform: An accurate technique for analyzing electromagnetic transients on power system devices," *Int. J. Elect. Power Energy Syst.*, vol. 31, no. 2–3, pp. 116–123, Feb./Mar. 2009.
- [10] A. Tavighi, J. R. Martí, and J. A. Gutiérrez-Robles, "Comparison of the fdLINE and ULM frequency-dependent EMTP line models with a reference Laplace solution," in *Proc. Int. Conf. on Power Systems Transients (IPST'15)*, Cavtat, Croatia, 15–18 Jun. 2015.
- [11] J. Martí and A. Tavighi, "Frequency-dependent multiconductor transmission line model with collocated voltage and current propagation," *IEEE Trans. Power Del.*, vol. 33, no. 1, pp. 71–81, Feb. 2018.
- [12] D. J. Wilcox, "Numerical Laplace transformation and inversion," *Int. J. Elect. Eng. Educ.*, vol. 15, no. 3, pp. 247–265, Jul. 1978.
- [13] L. M. Wedepohl, "Power system transients: Errors incurred in the numerical inversion of the Laplace transform," *26th Midwest Symposium on Circuits and Systems*, pp. 174–178, Aug. 1983.
- [14] A. Ramirez, P. Gómez, P. Moreno, and J. A. Gutiérrez-Robles, "Frequency-domain analysis of electromagnetic transients through the numerical Laplace transforms," in *Proc. PES General Meeting Conf. (PESGM'04)*, Denver, USA, 6–10 Jun. 2004, pp. 1136–1139.
- [15] P. Moreno and A. Ramirez, "Implementation of the numerical Laplace transform: A review," *IEEE Trans. Power Del.*, vol. 23, no. 4, pp. 2599–2609, Oct. 2008.
- [16] A. Tavighi, J. R. Martí, V. A. Galván, and J. A. Gutiérrez-Robles, "Time-window-based discrete-time Fourier series for electromagnetic transients in power systems," *IEEE Trans. Power Del.*, vol. 33, no. 5, pp. 2551–2561, Oct. 2018.
- [17] A. Tavighi, H. Ahmadi, M. Armstrong, and J. R. Martí, "Optimal phasing for parallel transmission lines to minimize AC interference," in *Proc. IEEE Canadian Conf. Elect. Comp. Eng. (CCECE'18)*, Québec City, Canada, 13–16 May 2018.
- [18] A. Tavighi, J. R. Martí, V. A. Galván, J. A. Gutiérrez-Robles, and H. W. Dommel, "A discrete time Fourier series formulation to simulate electromagnetic transients for multiconductor transmission lines," in *Proc. PES General Meeting Conf.*, Portland, USA, 5–9 Aug. 2018.
- [19] A. Tavighi, "A frequency-dependent multiconductor transmission line model with collocated voltage and current propagation," Ph.D. dissertation, University of British Columbia, Mar. 2017.
- [20] H. Ahmadi, M. Armstrong, and A. Tavighi, "Quantifying the shielding effect of trees against lightning strikes for power transmission lines," in *Proc. IEEE Canadian Conf. Elect. Comp. Eng. (CCECE'18)*, Québec City, Canada, 13–16 May 2018.